Reconstruction of the formation history of the Darwin Mounds, N Rockall Trough: How the dynamics of a sandy contourite affected cold-water coral growth

CrossMark

Lissette Victorero [a,b,*], Dominique Blamart [c], Edwige Pons-Branchu [c], Mark N. Mavrogordato [d], Veerle A.I. Huvenne [b]

[a] Ocean & Earth Science, University of Southampton, European Way, Southampton, UK
[b] Marine Geoscience, National Oceanography Centre, University of Southampton Waterfront Campus, European Way, Southampton SO14 3ZH, UK
[c] LSCE, Laboratoire CNRS-CEA-UVSQ, Domaine du CNRS, bat12, 91198 Gif sur Yvette, France
[d] μ-VIS CT Imaging Centre, Engineering Sciences, University of Southampton, Southampton SO17 1BJ, UK

ARTICLE INFO

ABSTRACT

Cold-water coral mounds, formed through a feed-back process of cold-water coral growth and sediment baffling, have been studied all along the NE Atlantic continental margin. However, major questions remain concerning their formation history, especially their initiation and early development in relation to the surrounding sediment dynamics. For the first time, two small mounds located in a sandy contourite have been cored from the top to mound base: here, the formation history of the Darwin Mounds, located in the Northern Rockall Trough was investigated and reconstructed from two piston cores using a multidisciplinary approach. This consisted of CT-scanning for quantifying coral density changes with depth, grain-size analysis to obtain the hydrodynamic trends and radiocarbon and U-series dating to place the results into a wider paleoceanographic context. The results show that the Darwin Mounds formed during the early Holocene (~10 ka BP) through sediment baffling, mainly by Lophelia pertusa. The initiation of both mounds shows a similar pattern of increased current velocities resulting in coarser sediment deposition and a relatively high coral density with a peak of 23 vol%. The mound growth was rapid between ~10–9.7 ka BP (up to 277 cm ka^{-1} in one of the mounds), with further vibrant growth periods around ~8.8 ka BP, 6.5 ka BP and 3.4 ka BP. The demise of the mounds ca. ~3 ka BP was likely caused by an intensification in bottom current velocities causing a hostile environment for coral growth in the contourite setting. In a wider context, the development of the Darwin Mounds appears to have responded to the relative strength and position of the Subpolar Gyre, which affected food supply to the corals, sedimentation rates, current speeds and other water mass properties in the area.

1. Introduction

Cold-water corals (CWC) are azooxanthellates (i.e coral species lacking photosynthesizing dinoflagellates) that thrive in water depths beyond the photic zone. The most intensely studied CWC species are the scleractinians Lophelia pertusa and Madrepora oculata. The distribution of these species is associated with a) increased surface primary productivity (Van Oevelen et al., 2009), b) water temperatures between 4 and 14 °C (Roberts et al., 2006; Freiwald, 2009), c) an aragonite saturation $\Omega_{aragonite}$ > 1 (Davies and Guinotte, 2011), d) a narrow potential density envelope (27.35–27.65 kg m^3) in the North-Atlantic (Dullo et al., 2008) and e) the correct substrate for larval settlement.

Furthermore, both species thrive in moderately high energy environments where they are supplied with food particles by a variety of hydrographies, such as currents, internal tides and downwelling flows (White, 2007; Davies et al., 2009). Lophelia pertusa and M. oculata can form structures ranging from patchy colonies to extensive multidimensional reef frameworks hence providing habitat for many species (Roberts et al., 2006, 2009, Henry et al., 2013). Over geological timescales cyclical reef growth combined with sedimentation and erosion can lead to CWC mound formation (Dorschel et al., 2007a; De Haas et al., 2009).

The formation and development of CWC mounds has been attributed to a variety of environmental factors affecting coral growth and sedimentation patterns. These include, among others, variations in oceanographic parameters induced by climatic changes. Changes in water-mass properties resulting in fluctuations in primary productivity and changes in mechanisms, such as density gradients and current

* Corresponding author at: Ocean & Earth Science, University of Southampton, European Way, Southampton, UK.
E-mail address: lvg1e12@soton.ac.uk (L. Victorero).

speeds, which affect the distribution of food particles, eventually lead to either increased or reduced food availability for the corals hence affecting mound growth.

The importance of studying CWC mounds lies in using them as potential paleoarchives. Their longevity combined with comprehension of environmental variables affecting CWC growth can provide information about past large-scale oceanographic processes that are affected by changes in the climate (Frank et al., 2009, 2011; Colin et al., 2010; Raddatz et al., 2014). Often CWC mounds are the only recorders of paleo-environmental signals in a given area, as the surrounding sediment record is too compressed or simply eroded away, due to fast bottom currents (Thierens et al., 2013). Furthermore, understanding the response of CWCs to environmental changes in the past is pivotal in identifying current and future threats to CWC habitats, which are identified as of high ecological value (Van Oevelen et al., 2009; Henry et al., 2013).

CWC mounds are a prominent feature along the North-East Atlantic margin occurring in a variety of shapes and forms, ranging from a few meters high and tens of meters wide to 350 m high and 2 km wide (Wheeler et al., 2007). The Darwin Mounds, located in the northern Rockall Trough (Fig. 1), consist of over 300 small individual mounds, up to 5 m high and 75 m across. These mounds, along with the Moira Mounds in the Porcupine Seabight, are considered unique as here *L. pertusa* and *M. oculata* grow on a contourite sand sheet, with many of the Darwin Mounds having downstream scoured tails of up to 500 m length (Masson et al., 2003; Huvenne et al., 2009a). Previously, the formation of the small mounds and a field of associated pockmarks of similar size were attributed to the escape of pore water from subsurface sediments creating elevated coarse-grained substrates that would become colonized by coral species (Masson et al., 2003). Conversely, Huvenne et al. (2009a) observed coinciding mineralogical characteristics between the mounds and the surrounding seabed. This gave rise

to a model in which the formation of the Darwin Mounds is caused by the local hydrodynamics supplying sediments that are entrapped by the partially permeable coral framework. The entrapped sediments remained protected from erosion, and over time accumulated leading to mound formation (Dorschel et al., 2007b; Wheeler et al., 2008; Huvenne et al., 2009a).

Unlike the present study, previous cores in the area have not penetrated through the base of a mound, which is essential for understanding the causal processes influencing mound initiation and hence understanding the paleoenvironment during subsequent formation and development. Here we investigated the formation history of two mounds from the Darwin Mounds province by quantifying changes in coral density and obtaining information on the hydrodynamics through time in two piston cores. In addition, dating of 14 selected coral fragments revealed sustained growth periods and coral hiatuses and permitted linking the formation history of the Darwin Mounds with the region's paleoenvironmental context.

2. Oceanographic setting

The dominant water mass in the Rockall Trough is the Eastern North Atlantic Water (ENAW) (Holliday et al., 2000) with the strongest flow present in the upper water column down to 500 m. There is also an inflow of the Modified North Atlantic Water (MNAW) which is transported by the North Atlantic Current (NAC), which flows towards the north-east. Along the eastern slope of the Trough, the Continental Slope Current (CSC) carries the ENAW northwards (Ellett et al., 1986). Both the ENAW and the CSC have been recorded to reach depths of 1000–1200 m (Ellett et al., 1986). The lower part of the CSC flows over the Darwin Mounds due to deflection by the Wyville Thomson Ridge (WTR) (Masson et al., 2003).The WTR also acts as a barrier preventing deep-water outflow from the Norwegian Sea entering the
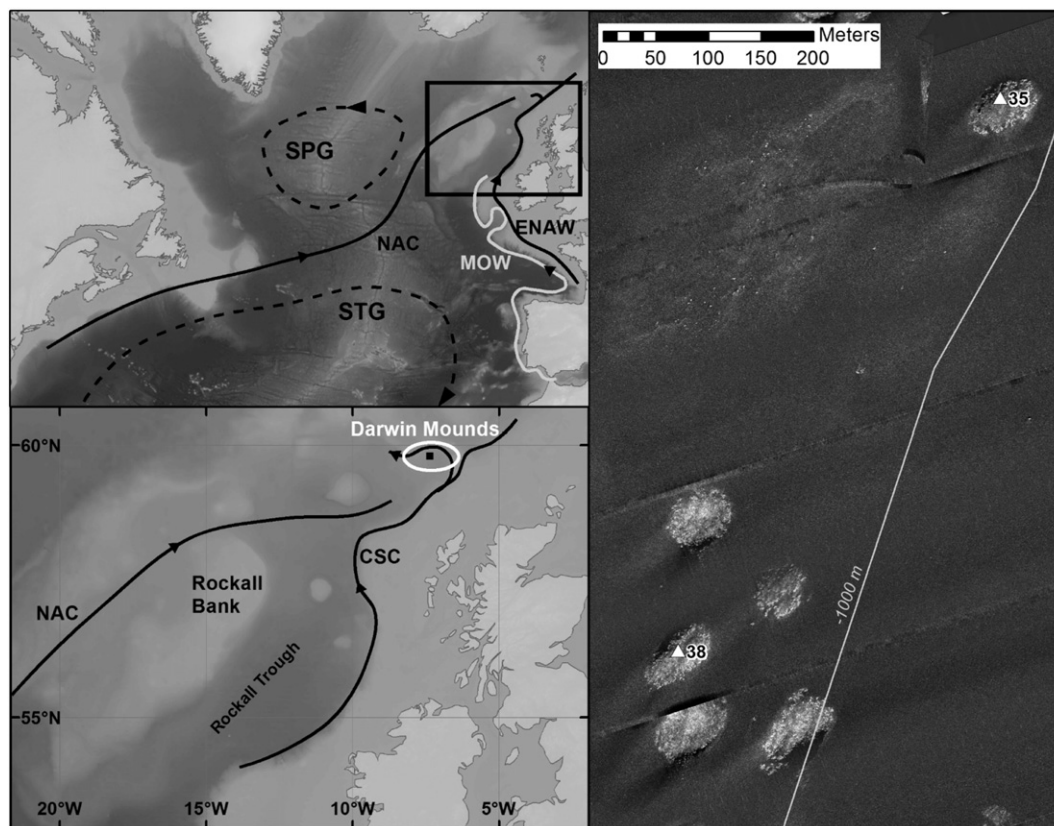

Fig. 1. Location map of the Darwin Mounds and the main water-masses and surface currents of the area, with sidescan sonar backscatter images illustrating coring locations through two small mounds. ENAW- Eastern North Atlantic Water, MNAW - Modified North Atlantic Water, MOW — Mediterranean Outflow Water, NAC — North Atlantic Current, SPG — Subpolar gyre, STG — Subtropical gyre. Background bathymetry is based on Smith and Sandwell, 1997 and the oceanographic illustration has been modified from Colin et al. (2010).

Trough (Hansen and Osterhus, 2000). The current meter data obtained in the area of the Darwin Mounds shows maximum near-bottom current speeds of ~35 cm/s with CTD casts measuring temperatures between 7.8–8.5 °C. (Masson et al., 2003).

3. Methodology

3.1. Core collection and imaging

In 2011 two piston cores were obtained through the bases of two separate Darwin Mounds (Fig. 1) during the expedition JC060 on board the RRS James Cook (Huvenne, 2011). The detailed location for both cores is shown in Table 1. The cores were frozen due to their high liquid content and were imaged in this state at the μ-Vis facility of the University of Southampton using X-ray Computerized Tomography (CT), which allowed for a non-destructive visualization, characterization and quantification of the CWCs present. The μ-CT images were acquired using a custom built, dual source 225/450 kV walk in room (Nikon Metrology, UK). The scans were acquired using the microfocus 450 kV source fitted with a tungsten reflection target together with a Perkin Elmer XRD 1621 CN03 HS detector. The scan settings used were: 210 kVp, 587 μA, 250 ms exposure, 3142 projections acquired during a full 360° rotation using an average of 2 frames per projection. The source-to-object distance was set at 348 mm with a source-to-detector distance of 803 mm – resulting in a 86.6 μm reconstructed voxel resolution. A 4 mm copper pre-filtration was used in addition to 2 mm thick aluminum window that forms part of the target housing. Reconstructions were performed using filtered back projection algorithms implemented within CTPro and CTAgent software packages (Nikon Metrology, UK). All image slices obtained from the scanning were processed using ImageJ (v.1.48) and 3D-images were created using the Volume Graphics Studio Max software package. In order to obtain the volume of coral and sediment from each slice, the images were filtered using a 3×3 median filter and then based on value (set point in a coral fragment) a threshold was applied to obtain a boundary between coral and surrounding sediment. The number of pixels obtained from the threshold were then multiplied by the voxel size (86.6 μm)^3 to obtain a coral volume. As this method is partly based on expert interpretation of the CT images, the threshold selection is somewhat subjective, but it aimed to exclude carbonate sediments and other $CaCO_3$ organisms. Unfortunately this can also underestimate the total coral volume calculations as it excludes small fragments (<0.5 mm) that cannot be identified as coral. The CT-scan images illustrated different coral species, hiatuses of coral growth, preservation status (bioerosion) and orientation of fragments indicating whether they were buried in situ or fragmented and later buried. Following the CT scanning, the cores were halved to ~50 cm lengths in their frozen state and split using a traditional rock saw. The cores were then allowed to thaw before sampling for dating and sediment-grain size analysis.

3.2. Coral dating

A total of 14 coral fragments were dated to establish when the Darwin Mounds were initiated and to place the coral density and grain-size results in to a regional paleoceanographic context. The selection of fragments was based on observed changes in the hydrodynamic

Table 1
Details of the piston cores from the Darwin Mounds.

Core number	Longitude	Latitude	Depth (m)
JC060-035	59° 49′.398 N	07° 21′.038 W	956
JC060-038	59° 49′.104 N	07° 21′.378 W	961

regime and/or marked changes in coral density. Four fragments were dated with radiocarbon at Beta Analytic Inc. (USA) and ten with uranium and thorium isotopes at the Laboratoire des Sciences du Climat et de l'Environnement in Gif-sur-Yvette (France). The radiocarbon analysis was conducted using the Accelerator Mass Spectrometer technique. The $^{13/12}$C ratios were measured by Isotope Ratio Mass Spectrometry and reported relative to PDB. The radiocarbon values were then corrected for isotopic fractionation using the equation $\delta^{13}C_{VPDB}$‰-25 using the ^{13}C values obtained through the process. Calibrations were conducted using the IntCal13 and Marine13 databases (Reimer et al., 2013).

Coral samples for U/Th were cleaned following methods described in Frank et al. (2004). The samples were first briefly cleaned in an ultrasonic bath and rinsed several times with distilled water at room temperature to remove detrital particles. Then the outermost surface of the corals was carefully ground to avoid remains of organic tissue and surface contaminants. This first mechanical cleaning was followed by a weak sanding treatment, an ultrasound treatment and additional rinses with milli-Q water. After adding the triple ^{229}Th ^{233}U-^{236}U spike in a Teflon beaker, the cleaned samples were dissolved with diluted HCl. The U and Th fractions were separated using UTEVA resin (Eichrom Technologies, Horwitz et al., 1998), following the procedure slightly modified from Douville et al. (2010). For half of the samples, uranium and thorium isotopes were determined simultaneously using a Thermo Fisher Scientific X series II ICPQMS coupled with the apex desolvating nebulizer system (Quad) following the procedure described in Douville et al. (2010). For 8 samples, including 2 replicates from the Quad analysis, uranium and thorium isotopes were determined simultaneously using a ThermoScientific Neptune^{Plus} multicollector-ICP-MS following the procedure described in Pons-Branchu et al. (2014). After corrections for peak tailing, hydrate interference and chemical blanks, age calculations from the isotopic data were conducted, based on iterative age estimation. Ages were corrected assuming an initial activity ratio of ^{230}Th/^{232}Th = 10 ± 4, based on the thorium ratio determined in North-Atlantic seawater (Moran et al., 1995; Vogler et al., 1998), which has also previously been used for coral age corrections in the area (e.g. Frank et al., 2004). All dates were used to estimate Vertical Mound Growth Rates (VMGR) for the individual mounds, which can function as a descriptor of the environmental regime. Assuming linear sedimentation rates between the dates, a conservative estimation of the growth rate can be calculated.

3.3. Sediment grain-size analysis and hydrodynamic regime

In order to understand the hydrodynamic regime of the mounds, the interaction between sediment transport and coral density, and to reconstruct how this impacted mound formation through time, sediment grain-size analysis was conducted on the terrigenous fraction. Sediment samples (~0.5 cm^3) were collected at 25 cm intervals along both cores with additional sampling points at boundaries where the sediment type was considered to change more abruptly. The samples were treated with H_2O_2 and HCl to remove all organic matter and calcium carbonate respectively. Prior to analysis 20 ml of 0.05% $(NaPO_3)_6$ dispersant solution was added to the samples, which were left to shake overnight. The sediment grain-size was measured using a Malvern Mastersizer 2000 laser diffraction particle size analyzer.

The modes of the resulting grain-size distribution curves, for those samples where they fell into the sand fraction (>63 μm), were used to estimate of the critical current velocity 1 m above the seabed which would be required to move the sediments, and the critical current velocity under which the sediment grains would settle from the water column. By comparing which variable is higher, it was estimated whether settling or transport by saltation occurred at the moment of deposition at the sampling points. The calculations provided an insight into changes in current velocities over time in the mounds. The equations, specifically designed for mobile sands, are based on Soulsby (1997),

with mathematical detail explained in Huvenne et al. (2009a). Below we introduce briefly the two main equations used for this study. The critical current velocity required for erosion 1 m above the seabed can be calculated as follows:

$$u_{100 \text{ erosion}} = \left(\frac{u_{*cr}}{0.41}\right) \ln\left(\frac{z_{100}}{z_0}\right), \text{ where} \tag{1}$$

$$z_{100} = \text{level above seabed (1 m)} \tag{1.1}$$

$$z_0 = \text{roughness length, calculated} = \left(\frac{d}{12}\right) \tag{1.2}$$

$$d = \text{grain diameter} = \text{mode of sample grain size curve} \tag{1.2.1}$$

$$u_{cr} = \text{critical shear velocity} = u_{*cr} = \sqrt{\frac{\tau_{cr}}{\rho}}, \text{ where} \tag{1.3}$$

$$\tau_{cr} = \text{threshold bed shear stress}\left(\text{N/m}^2\right) = \tag{1.3.1}$$

$$g(\rho_s - \rho)d.\left(\frac{0.30}{1 + 1.2D_*} + 0.055[1 - \exp(-0.020D_*)]\right) \tag{1.3.1}$$

$$\rho = \text{water density} = 1027.4 \text{ kg/m}^3 \tag{1.3.2}$$

$$\rho_s = \text{grain density} = 2650 \text{ kg/m}^3 \text{ (quartz)} \tag{1.3.3}$$

$$D_* = \text{dimensionless grain size} = \left[\frac{g(\rho_s - \rho)}{\rho v^2}\right]^{\frac{1}{3}} d \tag{1.3.4}$$

The settling velocity of a grain was calculated as follows

$$u_{\text{setl}} = \frac{v}{d}\left[\left(10.36^2 + 1.049D_*^3\right)^{\frac{1}{2}} - 10.36\right], \text{ where} \tag{2}$$

$$v = \text{kinematic viscosity of water} = 1.4313 \\ \times 10^{-6} \text{ m}^2/\text{s (8 °C and 35.1 ppt)} \tag{2.1}$$

4. Results

4.1. Analysis of CT-scan data

From the CT-scan image data it is clear that the main coral species participating in the formation of the Darwin Mounds was *L. pertusa*. This species occurs throughout the cores in a chaotic orientation embedded in the sediment matrix, with no apparent attachment to firm substrata. Other species present include *M. oculata*, which occurs in both cores generally as a few scattered fragments mixed in with *L. pertusa*, and to a lesser extent the solitary coral *Desmophyllum* sp. (Fig. 2).

Changes in coral density throughout both cores are presented in Figs. 3 and 4. The two cores show slightly different density trends. In core 035 coral density values range between 0 and 19% with peak values reached more towards the top of the core (19% at ~110 cm and ~15% at ~60 cm and ~40 cm). In core 038 the coral densities range from 0 to ~23%. Peak values (>15%) in this core occur at the depths of ~260, 135 and ~60 cm (Figs. 4 and 5, A). Intervals of relatively low coral density (0–3%) occur at 150–175 cm and 8–25 cm. Fluctuations in coral density leading to coral hiatuses is also apparent (Fig. 5, B). Towards the top of both cores there is an increase in coral density in the form of coral rubble.

In core 035, *M. oculata* appears for the first time at the depth of 188 cm, while in core 038 it is observed for the first time at the much deeper depth of 280 cm (Figs. 3 and 4). In core 035, at 88 cm depth, *M. oculata* occurs at its highest density throughout the study and is also as the main coral species present at this depth. *Desmophyllum* sp. is absent from core 035, but appears in core 038 at the depth of 230 and 126 cm. Bioerosion of the corals was visible in the images and was visually verified during core splitting. The first bioeroded coral appears in core 038 at the depth of 258 cm. In both cores a general trend of increasing bioerosion towards the top can be observed (Figs. 3 and 4). The images also show preservation of various gastropod species.

4.2. Coral dating

Dates obtained from *L. pertusa* specimens in core 035 and 038 (Tables 2 and 3), suggest that mound growth initiated around ~10 ka
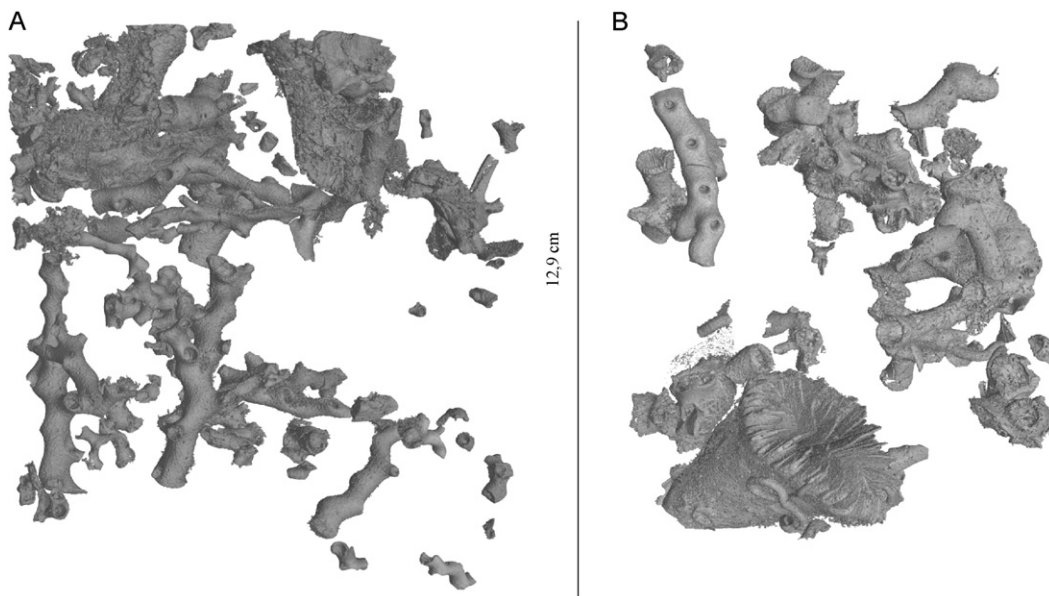

Fig. 2. CT-scan image illustrating different coral species in 3D. A: an abundant *Madrepora oculata* image slice from core 035 at 88 cm depth and B: the solitary coral *Desmophyllym sp.* from core 038 at 231 cm depth.
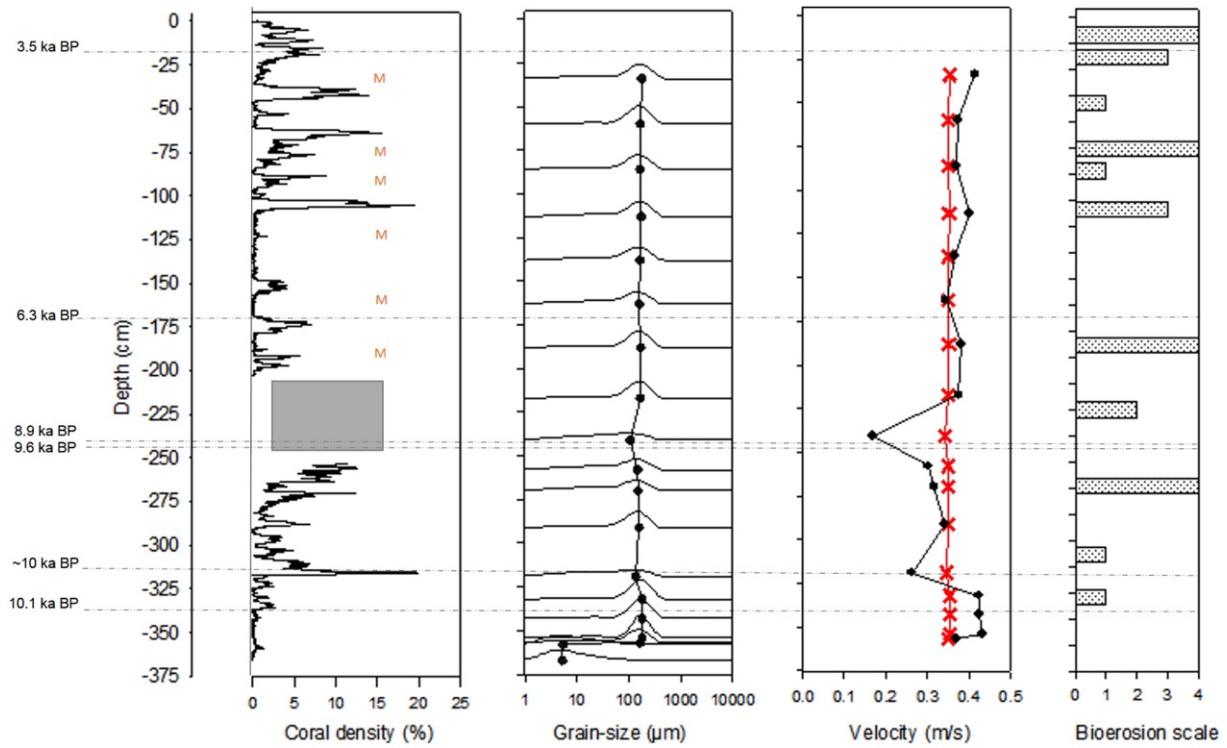
Fig. 3. Panel of graphs illustrating parameters measured from core 035 with dates. The letter M in the coral density plot illustrates the presence of *Madrepora oculata*. Gray box indicates core segment that failed to be successfully CT-scanned. The black dots indicate sampling points for grain-size analysis. The red line in the velocity graph indicates a threshold between sediment deposition occurring by suspension or saltation with high velocities resulting in saltation. The bioerosion scale is a visual nominal scale, ranging from 0- no bioerosion to 4- heavily bioeroded.
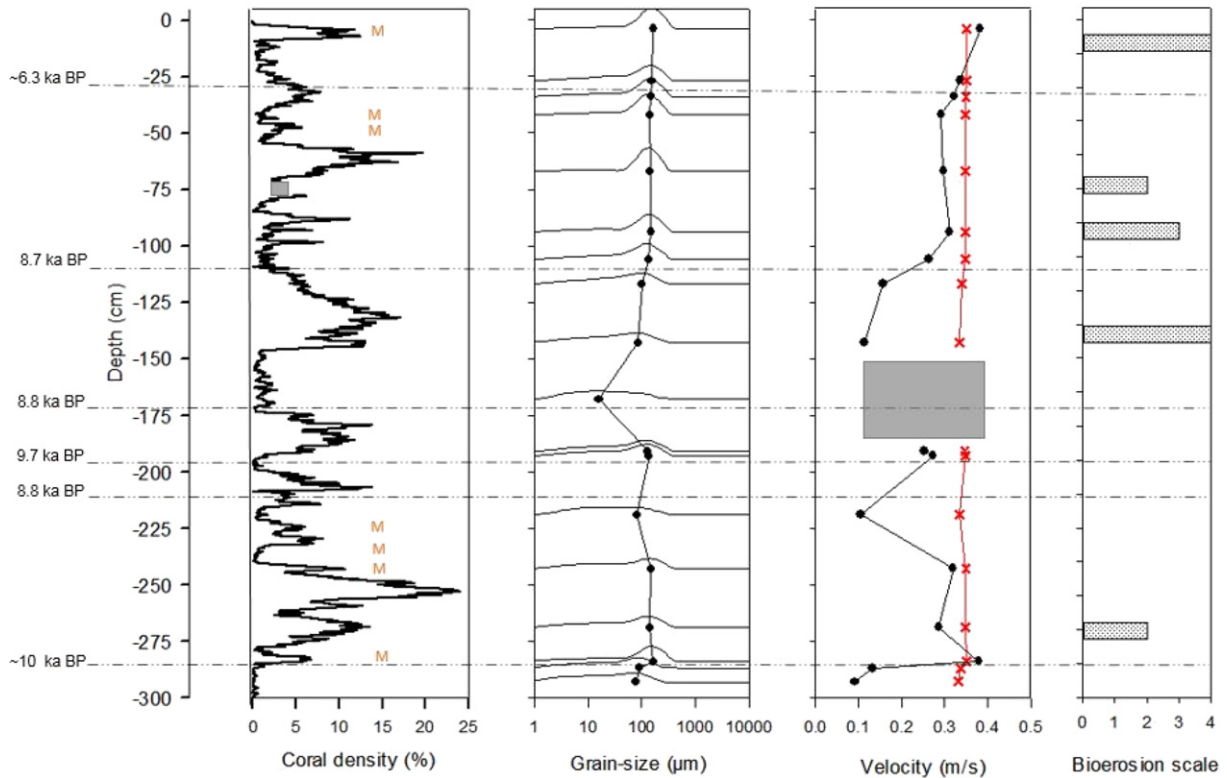

Fig. 4. Panel of graphs illustrating parameters measured from core 038 with dates. The letter M in the coral density plot illustrates the presence of *Madrepora oculata*. Gray box indicates core segment that failed to be successfully CT-scanned. The black dots indicate sampling points for grain-size analysis. The red line in the velocity graph indicates a threshold between sediment deposition occurring by suspension or saltation with high velocities resulting in saltation. Gray box indicates modes that were too low for erosional velocity calculations. The bioerosion scale is a visual nominal scale, ranging from 0- no bioerosion to 4- heavily bioeroded.
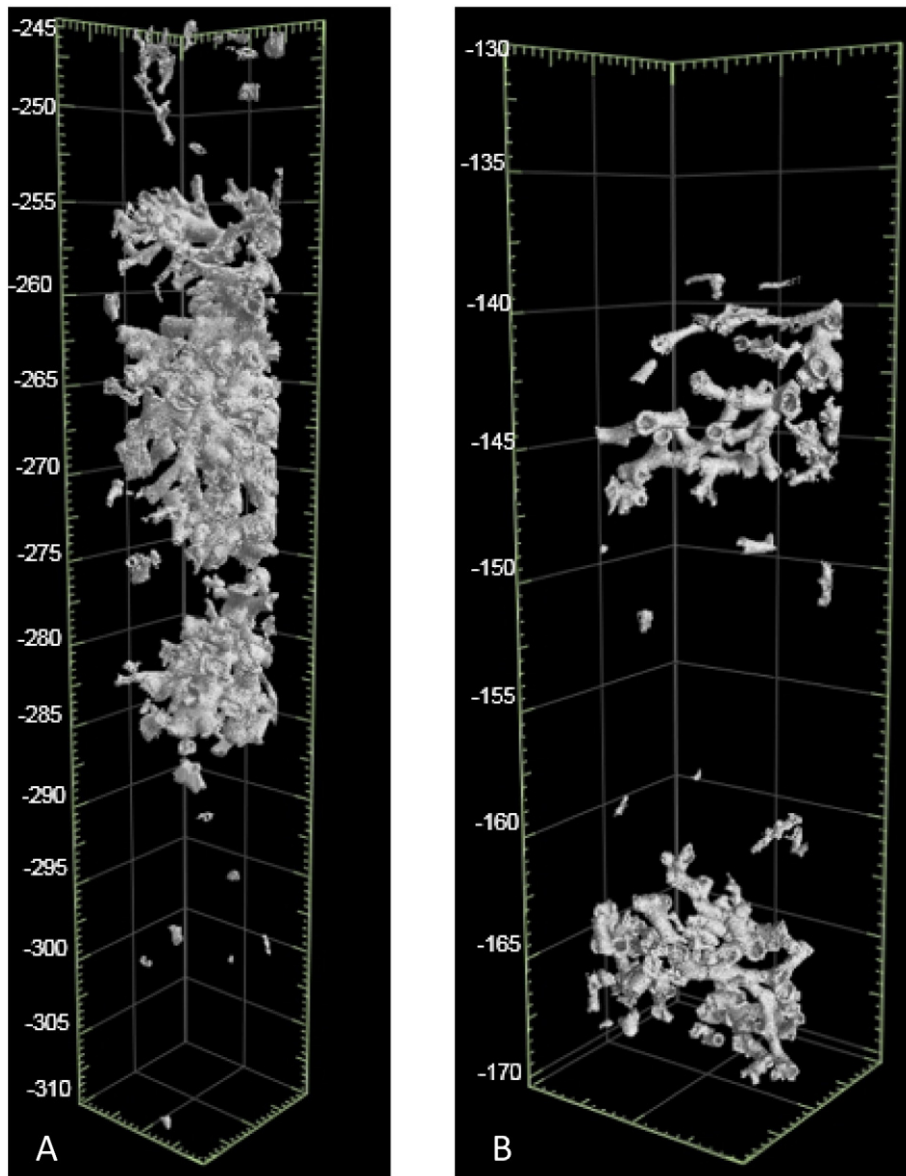
Fig. 5. CT-scan images illustrating A: the mound base from core 038 with high coral density and B: variation in coral density and coral hiatuses in core 035. The scale represents the relative depth in the core in cm.

Table 2
The age of selected *Lophelia pertusa* fragments from the cores based on U-series dating. Repeated measurements are from the same fragment. The method describes the instrument used for measurements.

Sample Name	Depth in core (cm)	^{238}U (µg/g)	^{238}U (µg/g)	$\delta^{234}U_m$	^{230}Th/^{232}Th	^{230}Th/^{238}U	$\delta^{234}U_{(0)}$	Method	Age (ka BP)
038-S2-19-outer	−28	3.649 ± 0.007	0.83 ± 0.004	144.7 ± 0.6	1024.8 ± 3.7	0.0693 ± 0.0003	147.5 ± 0.6	Neptune	6.68 ± 0.05
038-S2-19 -inner	−28	4.025 ± 0.005	0.70 ± 0.003	143.6 ± 1.2	1186.9 ± 7.9	0.0659 ± 0.0004	146.2 ± 1.2	Neptune	6.35 ± 0.07
038-S2-19 -inner	−28	4.095 ± 0.013	0.64 ± 0.003	139.3 ± 5.2	1205.9 ± 33.6	0.0616 ± 0.0017	141.7 ± 5.3	Quad	5.95 ± 0.22
0S38-S2-19	−28	3.776 ± 0.003	0.59 ± 0.001	146.1 ± 1.2	1240.5 ± 5.1	0.0636 ± 0.0003	148.7 ± 1.2	Neptune	6.12 ± 0.05
038-S2-101	−110	3.358 ± 0.003	0.74 ± 0.005	144.7 ± 0.6	1347.1 ± 8.7	0.0894 ± 0.0006	148.3 ± 0.6	Neptune	8.73 ± 0.09
038-S3-60	−170	4.050 ± 0.015	0.78 ± 0.006	140.9 ± 5.6	1389.0 ± 32.5	0.0886 ± 0.0020	144.4 ± 5.7	Quad	8.69 ± 0.27
038-S3-80	−190	3.223 ± 0.007	1.58 ± 0.008	136.5 ± 4.9	610.2 ± 11.0	0.0981 ± 0.0017	140.3 ± 5.1	Quad	9.63 ± 0.28
038-S3-80	−190	3.165 ± 0.004	1.79 ± 0.005	144.1 ± 1.1	564.3 ± 2.2	0.0983 ± 0.0004	148.1 ± 1.1	Neptune	9.57 ± 0.12
038-S3-97	−207	3.853 ± 0.013	0.48 ± 0.004	142.9 ± 5.3	2168 ± 91.9	0.0894 ± 0.0037	146.5 ± 5.4	Quad	8.78 ± 0.44
038-S4-75	−285	3.915 ± 0.004	1.11 ± 0.014	143.9 ± 0.7	1235.4 ± 8.2	0.1044 ± 0.0007	148.2 ± 0.8	Neptune	10.28 ± 0.11
038-S4-75	−285	3.847 ± 0.010	0.58 ± 0.001	143.5 ± 1.0	2090.0 ± 4.1	0.1033 ± 0.0002	147.7 ± 1.0	Neptune	10.21 ± 0.05
035-S2-70	−173	3.801 ± 0.010	2.13 ± 0.001	144.0 ± 0.9	371.7 ± 0.4	0.0664 ± 0.0001	146.6 ± 1.0	Neptune	6.29 ± 0.08
035-S2-70	−173	4.058 ± 0.004	2.88 ± 0.008	145.4 ± 0.9	312.0 ± 1.5	0.0660 ± 0.0003	148.0 ± 0.9	Neptune	6.20 ± 0.12
035-S3-26	−234	3.452 ± 0.003	1.10 ± 0.007	144.8 ± 0.6	1035.8 ± 7.0	0.0980 ± 0.0007	148.8 ± 0.6	Neptune	9.60 ± 0.11
035-S3b-111	−319	3.338 ± 0.011	0.55 ± 0.005	141.5 ± 4.0	1845.5 ± 48.0	0.1007 ± 0.0025	145.5 ± 4.2	Quad	9.95 ± 0.32
035-S3b-111	−319	3.276 ± 0.003	0.65 ± 0.003	144.3 ± 0.9	1623.2 ± 8.5	0.1027 ± 0.0005	148.5 ± 1.0	Neptune	10.13 ± 0.09

^{234}U/^{238}U ratios are expressed as: $\delta^{234}U = ([^{234}U/^{238}U]_{activity} - 1) \times 1000$.

Table 3
Radiocarbon dates from selected *Lophelia pertusa* fragments.

Sample Name	Depth in core (cm)	δ¹³C (‰)	Conventional radiocarbon age (ka BP)	Calibrated age (ka BP)	Calibrated age-range (±2σ –95% probability) (ka BP)
038-S4-75	−285	0.2	9.190 ± 40	10.000	9.840–10.148
035-S1-17	−17	−5.1	3.640 ± 30	3.541	3.446–3.630
035-S3-26	−234	−6.4	8.300 ± 40	8.862	8.701–8.987
035-S4-08	−332	−3.9	9.290 ± 40	10.138	9.992–10.219

BP. The age of 9.6 ka BP in the stratigraphic sequence of core 035 coincides with a change towards finer sediment-grain size and is followed by trend of reduced coral density. The dates of 6.3 ka BP represent a brief coral growth period while 3.5 ka BP marks the end of the final growth period. The majority of dates from core 038 fall between 10.1–8.7 ka BP with several age reversals occurring. The last date acquired of 6.5 ka BP indicates the last period of sustained and well-preserved coral growth as the high coral density recorded after this consists of highly bioeroded coral rubble, suggesting a collapse of the coral framework.

The VMGR values range between 18 and 277 cm ka⁻¹ for core 035 and 20–199 cm ka⁻¹ for core 038. A pronounced growth period of 91–277 cm ka⁻¹ occurred at the beginning of core 035 with another relatively high accumulation rate present between 6.3–3.5 ka BP (Fig. 6). Extrapolation suggests that mound growth finished around 3 ka BP. Similarly, in core 038, the highest VMGR occurs towards the base, between 190 and 285 cm depth (199 cm/ka⁻¹) with the lower vertical accumulation rates (49 cm ka⁻¹) present after ~8.7 ka BP and mound growth ceasing ~6 ka BP. It must be noted, however, that the limited amount of dates available from core 038 adds extra uncertainties to the VMGR calculations.

4.3. Sediment grain-size analysis

The sediment grain-size analysis of the terrigenous fraction shows a general coarsening trend from the bottom to the top in both mounds (Figs. 3 and 4). In core 035 the modes range from 5 μm at the bottom of the core to 178 μm at 343 cm depth. A sharp increase in the mode value (from 5.4 μm to 162.6 μm) occurs closer to the bottom of the core (mound base), notably below the occurrence of the first coral fragment between 357 and 358 cm (Fig. 3). The mode value also decreases abruptly to 105 μm at 241 cm depth. This is followed by another abrupt increase with the next data point (217 cm depth) having a value of 164 μm from which onwards the mode values remain quite constant until the top of the core.

Core 038 has a more complex sediment grain-size pattern (Fig. 4). The modes range from 16.1 μm (168 cm depth) to 166 μm at the very top of the core. The bottom of the core has a mode value of 76.2 μm, which increases in the 243–293 cm interval, together with the appearance of the first coral fragment, reaching 149 μm. In the next successive data point a large drop in the mode value, similarly to core 035, can be observed (81 μm) which is then followed by an increase up to 137 μm (191–193 cm). This is again followed by an abrupt drop down to 16.1 μm (168 cm). From this point onwards the mode steadily increases from 80 μm towards the top reaching the maximum value of 166 μm.

4.4. Hydrodynamic interpretation

The action of sand grains in the water column for the majority of core 035 can be described as saltating, since the critical erosion velocity < settling velocity (Fig. 3). The exceptions for this are between 320 and 240 cm depth, where the erosional velocity is higher than the settling velocity indicating that the particles were transported in the water column and deposited through settling. At the approximate depth of 240 cm there is a marked reduction with the settling velocity reaching its minimum point of 0.17 m/s indicating low current activity. The grain activity suggests that currents were faster at the initiation of this mound and were then reduced for the period between 240 and 320 cm. Following this interval, the currents show a trend of acceleration.

In core 038 the majority of the sediments were deposited through settling, with the exception at 284 cm depth and at the top 4 cm (Fig. 4). The highest reduction in the settling velocity (down to ~0.10 m/s) occurs around 220 and 140 cm depth. There is also an abrupt decrease in the sediment-grain size at 170 cm, which was unsuitable for the current calculations. As such the core from this mound indicates slower currents for the majority of the time with sediment being deposited through settling throughout the mound's existence with the exception of the very top 4 cm.

5. Discussion

5.1. Reconstruction of the initial mound growth period: 10.2–9.6 ka BP

Lophelia pertusa started growing at the Darwin Mounds in the early Holocene around ~10 ka BP. These dates are in agreement with previously dated *L. pertusa* fragments from the south-west Rockall Bank, where coral growth re-started 12. 9–11.5 ka BP ago (Frank et al., 2009).
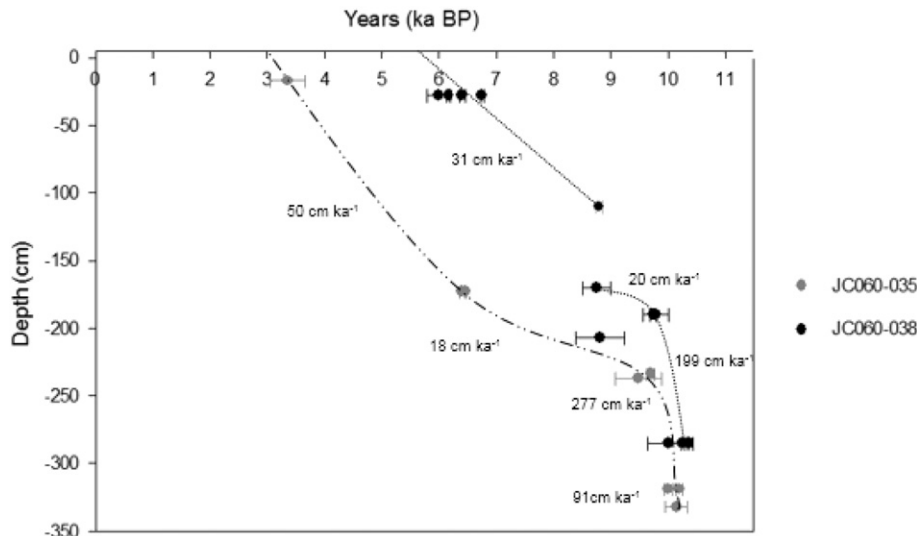

Fig. 6. The estimated Vertical Mound Growth Rate derived from the age (ka) − depth (cm) relationship showing growth rate periods for both cores.

Initial coral growth in the Darwin Mounds seems to have closely followed the acceleration of currents leading to the presence of coarser grained sediments and initiation of the sandy contourite sheet in the area. The existence of coral so briefly after the presence of coarser sediment rejects the hypothesis that the corals colonized elevated sandy mounds (Masson et al., 2003) but instead suggests they potentially settled on boulders or dropstones. In both mounds the highest VMGR is observed at the initiation phase between ~10–9.6 ka BP: 230 cm ka^{-1} and ~200 cm ka^{-1}, for core 035 and 038 respectively. These estimates exceed those from large CWC mounds on Rockall Bank with VMGR rates of 60 cm ka^{-1}, but are in agreement with Porcupine Seabight values (220 cm ka^{-1}, between 9.8–8.5 ka BP) (Frank et al., 2009) with such differences attributed to the sediment input being terrigenous at the Porcupine Seabight, while Rockall Bank is carbonate dominated (Van der Land et al., 2014).

Increasing coral density is specifically apparent in core 038, reaching the peak value throughout the study of 23% prior to 9.7 ka BP. Furthermore, the occurrence of few fragments dated ~9.6 ka BP in both cores also supports the interpretation of a prolific coral growth period around this time. Once present, coral framework and live coral colonies would have caused a reduction in current velocity and increased sediment settling on-mound (Masson et al., 2003). The results are also in accordance with previous work by Huvenne et al. (2009a), which suggested that mound growth is the result of sediment baffling by the coral species present as the sediment composition of the mounds does not differ greatly from the surrounding area.

5.2. Reconstruction of mound development: 9.6–3.5 ka BP

Following the period of initial mound growth, each core portrays a different development scenario. The mound of core 038 exhibits higher coral densities from the start which could potentially reflect sustained coral growth through positive feedback. Higher density colonies are likely to trap more sediment through reduction of current speed, which in turn would have provided support for the colonies allowing the mound to grow higher (Foubert et al., 2011). The presence of several fragments dated ~8.8 ka BP between 110 and 207 cm depth, even causing age-reversals, also suggests a vibrant coral growth in the mound during this time, interspersed with occasional collapses of large coral colonies. Similarly, in core 035 there is a fragment dated at 8.9 ka BP, but there is unfortunately no density data available for this time.

Based on granulometric data, a decrease in current velocity is present in both cores, but unfortunately the timing is unclear based on the dates obtained. This change is followed by reduced coral densities which indicate the start of an unfavorable environmental regime. Furthermore in core 038 there is an additional drastic alteration in the hydrodynamics at 170 cm coinciding with a coral hiatus. This increment of fine sediment deposition and slow currents resulted in a rapid burial of coral frameworks. This may explain the lack of bioerosion marks on the coral fragments despite the presence of an age reversal. Coinciding with the slower currents, there is the first appearance of a few M. oculata fragments in core 038. A coral age gap between 8.7–6.3 ka BP, comparable to gaps from the Rockall Bank and Porcupine Seabight (Frank et al., 2009), also exists.

A brief coral growth period is observed in both cores around 6.3–6 ka BP which is likely to have been spurred by an increment in current velocity resulting in a reduction of sediment deposition and potentially increased food input. Alterations between high and low peaks of coral density towards the top of both cores suggest that slight changes in current speed in the sandy contourite environment of the Darwin Mounds can have profound effects on the sediment behavior (Huvenne et al., 2009a). Coral growth appears to be impacted negatively both when there is a shift towards a faster current regime, most likely caused by coarse sediment causing abrasion and when the currents are very slow, causing deposition of fine material leading to smothering of coral.

Extrapolating the age-framework of core 038, it can be inferred that this mound ceased to grow around ~6 ka BP. The presence of medium coral densities at the top of the core, consisting of highly bio-eroded fragmented coral pieces, seems to indicate that sediment supply to and baffling by the mound had become minimal. The other mound, however, with its relatively faster currents appears to have had another short period of coral growth around 3.5 ka BP with mound growth ceasing around 3 ka BP. Similarly, in the Mingulay Reef Complex a major growth rate decline was observed at ~3.5 ka BP (Douarin et al., 2013). Additionally, spatial variability in the hydrodynamic properties between individual mounds in the Darwin mound has also been described before by Huvenne et al. (2009a).

Despite differing timings for the demise of the mounds, in both cases it seems to be partially driven by increased current velocities, beyond the optimal speed, over a longer time period, with visual changes in species composition and increased abundance of M. oculata, fragmented pieces of L. pertusa and rubble. In particular, the presence of M. oculata has been linked to mound demise in, for example, both the Challenger Mound (Foubert and Henriet, 2009) and the sediment-stressed Moira Mounds in the Porcupine Seabight (Foubert et al., 2011) as M. oculata appears to have higher flexibility with regard to environmental conditions (Wienberg et al., 2009). The smaller polyps of M. oculata are suggested to be more efficient in rejecting sediment, hence avoiding clogging better than the large polyped L. pertusa (Foubert et al., 2011).

Finally, it is worth noting that the coral densities in this study can be considered low in comparison, for example, to the Challenger Mound, where densities above 10% were continuously found over several intervals in the CT-scan data (Foubert and Henriet, 2009). It is admittedly controversial to compare the small Darwin Mounds to the giant Challenger Mound, which reaches ca. 80 m above seabed and has a total height of ~155 m. Still, it is clear that the Darwin Mounds are a much more sediment-dominated system. The obtained low density values throughout time and constant fluctuations in coral density are likely to reflect that there is a fine balance between sedimentation and erosion in the contourite environment. The low coral density could also indicate that corals in a sandy contourite environment are under pressure and not at their optimal conditions. The final demise of the mound from which core 035 was obtained, at 3 ka BP, could potentially suggest that in a sandy contourite environment it is harder and takes longer for coral colonies to recover from disadvantageous environmental conditions, such as lack of food and fast currents causing abrasion.

Despite the discussed demise, high-resolution sidescan sonar records (Wheeler et al., 2008) and ROV video surveys have shown live coral colonies from the Darwin Mounds (Howell et al., 2014). As seen from the backscatter (Fig. 1) live coral colonies also exist next to the coring location of 035, but further apart from core 038, which supports the different demise timings found in the study. Furthermore, these observations show that instead of coral growth stopping completely or corals disappearing, it is more likely that the coral density reduced significantly over time causing some mounds to become dormant. As the Darwin Mounds province is composed of over 300 small mounds, which show high spatial variability as discussed above, it is suggested that the coral colonies presently occurring at the site are a mixture of both older and younger coral.

Overall, small mounds, such as the Darwin and Moira Mounds, have been suggested to represent an early stage in giant CWC mound build-up with each individual mound representing a nucleation site (Wheeler et al., 2011). The fact that no sand facies was found at the base of the Challenger Mound questions this idea (Huvenne et al., 2009b). Alternatively, while the initiation of the mounds might not be related, the similar response to sediment stress in all of the three mound provinces could potentially suggest that over time, under an environmentally favorable regime, sustained for a long enough time, the Darwin Mounds could grow in to a giant CWC mound (Wheeler et al., 2011).

5.3. Mound growth in the region's paleoceanographic context

The environmental shift initiating the development of the Darwin Mounds is likely to have been caused by the warming climate after the Younger Dryas (YD) cold reversal dated back to 10.3 ka BP in the northern Rockall Through (Rasmussen et al., 2002). This warming lead to an enhanced primary productivity (Abrantes et al., 1998) which had a pivotal role in affecting coral growth in the North-East Atlantic. The interplay between the cold, fresher Subpolar Gyre (SPG) and more saline, warmer Subtropical Gyre (STG) and their relative position seems to also have had an effect on the subsequent mound development. Their relative position affected surface primary productivity (Johnson et al., 2013), the hydrodynamic regime and sedimentation rate over the northern Rockall Trough (Rasmussen et al., 2002). Furthermore, this interplay might also have stimulated larval transport through inflow of the Mediterranean Outflow Water (MOW) into the Porcupine Seabight (Lozier and Stewart, 2008) and potentially into the Rockall Trough (Colin et al., 2010). It has been suggested that a strong SPG would have shifted the subpolar front towards the east, allowing an interception of the NAC and allowing a flow consisting of a mixture of NAC and MOW to enter the Rockall Trough (Henry et al., 2014). As such, the MOW has been proposed to act as a transport pathway bringing *L. pertusa* larvae from the Mediterranean (De Mol et al., 2002, 2005), where intense coral growth occurred during the YD (McCulloch et al., 2010). With genetic work suggesting a close connection between the populations from the Mediterranean and the North-East Atlantic (Flot et al., 2013), coral growth in the Rockall Trough could be a result of an inflow episode of MOW as it is now known that *L. pertusa* larvae have high dispersal potential and are likely to survive more than 8 weeks (Larsson et al., 2014).

The neodymium isotopic composition (quasi-conservative water–mass tracer) obtained from *L. pertusa* and *M. oculata* specimens from the Rockall Bank/Rockall Trough area (Colin et al., 2010) suggests that during the 9.4–6 ka interval the SPG had a greater eastward extension entering the Rockall Trough, resulting in increased nutrient availability and enhanced primary productivity. This partly agrees with the results obtained here in which relatively high constant coral density can be observed till ~8.8 ka BP. There is a distinct change in sediment grain-size recorded in both cores reflecting an environmental change, however with discrepancy in the timing due to age-reversals. The coral age gap (8.7–6.3 ka BP) present here and in other data-sets might be linked to an abrupt cold period at 8.2 ka BP (Kobashi et al., 2007) or it could be speculated that a particularly strong SPG circulation does not provide the ideal circumstances for coral growth either.

Approximately at ~6 ka the SPG was displaced westward again and there was an increased inflow of the STG in to the Rockall Trough (Colin et al., 2010) leading to a reduction in nutrient inflow and surface primary productivity in the area (Johnson et al., 2013). This marks the last episode of coral growth in both mounds followed by the demise of one of the mounds. From here on, the SPG experienced cyclical strengthening and weakening till approximately 4 ka, followed by a progressive weakening till 0 ka (Staines-Urías et al., 2013), which is likely to be reflected in the observed coral density fluctuations in core 035 around 3.5 ka BP. The last dating also coincides with a particularly strong STG flow dated 3.6 ka (Colin et al., 2010). This potentially was the last adverse event leading to the final dormancy at 3 ka. The weakened SPG also increased in particular the lower flow of the ENAW (Staines-Urías et al., 2013), which is conceivably reflected in data from core 035 as there is a trend of increasing current velocities which are likely to cause physical discomfort to corals as discussed previously.

In summary, although this study has successfully placed the formation of the Darwin Mounds into the wider paleoceanographic context of the region, the variability between the cores reflects the necessity of further research, with additional cores, the acquisition of additional dates and perhaps the application of new proxies, such as neodymium to obtain detailed information on the oceanographical changes through time. Despite this, this initial study shows that the Darwin Mounds are relatively sensitive to environmental changes and can be used as paleoenvironmental recorders in this sandy contourite setting, where the off-mound sediment record for the same time period is too condensed and disturbed by constant erosion/deposition processes to provide the detailed information necessary to illustrate the climatic patterns of the region.

6. Conclusion

Coral growth in the Darwin Mounds started ~10 ka BP following the Younger Dryas cold reversal. The current study verifies that the mounds are formed through sediment baffling by coral framework. The mound growth was rapid until ~8.8 ka BP with another brief proliferation at ~6.3 ka BP. The combination of CT-scanning, sediment analysis and dating revealed that the hydrodynamic regime of the sandy contourite played an important role in coral growth with the demise of the mounds being linked to an intensification of the bottom current regime. The position and relative strength of the Subpolar Gyre and Subtropical Gyre are postulated to have affected nutrient input, sedimentation and bottom current speeds in the area affecting the development of the Darwin Mounds.

Acknowledgments

References

Abrantes, F., Baas, J., Haflidason, H., Rasmussen, T., Klitgaard, D., Loncaric, N., Gaspar, L., 1998. Sediment fluxes along the northeastern European margin: inferring hydrological changes between 20 and 8 kyr. Mar. Geol. 152, 7–23. http://dx.doi.org/10.1016/S0025-3227(98)00062-0.

Colin, C., Frank, N., Copard, K., Douville, E., 2010. Neodymium isotopic composition of deep-sea corals from the NE Atlantic: implications for past hydrological changes during the Holocene. Quat. Sci. Rev. 29, 2509–2517. http://dx.doi.org/10.1016/j.quascirev.2010.05.012.

Davies, A.J., Guinotte, J.M., 2011. Global habitat suitability for framework-forming cold-water corals. PLoS One 6, e18483. http://dx.doi.org/10.1371/journal.pone.0018483.

Davies, A.J., Duineveld, G.C.A., Lavaleye, M.S.S., Bergman, M.J.N., Van Haren, H., Roberts, J.M., 2009. Downwelling and deep-water bottom currents as food supply mechanisms to the cold-water coral Lophelia pertusa (Scleractinia) at the Mingulay Reef complex. Limnol. Oceanogr. 54, 620–629. http://dx.doi.org/10.4319/lo.2009.54.2.0620.

De Haas, H., Mienis, F., Frank, N., Richter, T.O., Steinacher, R., de Stigter, H., van der Land, C., van Weering, T.C.E., 2009. Morphology and sedimentology of (clustered) cold-water coral mounds at the south Rockall Trough margins, NE Atlantic Ocean. Facies 55, 1–26. http://dx.doi.org/10.1007/s10347-008-0157-1.

De Mol, B., Henriet, J.-P., Canals, M., 2005. Development of coral banks in Porcupine Seabight: do they have Mediterranean ancestors? Cold-Water Corals and Ecosystems. Springer Berlin Heidelberg, pp. 515–533

De Mol, B., Van Rensbergen, P., Pillen, S., Van Herreweghe, K., Van Rooij, D., McDonnell, A., Huvenne, V., Ivanov, M., Swennen, R., Henriet, J., 2002. Large deep-water coral banks in the Porcupine Basin, southwest of Ireland. Mar. Geol. 188, 193–231. http://dx.doi.org/10.1016/S0025-3227(02)00281-5.

Dorschel, B., Hebbeln, D., Foubert, A., White, M., Wheeler, A.J., 2007b. Hydrodynamics and cold-water coral facies distribution related to recent sedimentary processes at Galway Mound west of Ireland. Mar. Geol. 244, 184–195. http://dx.doi.org/10.1016/j.margeo.2007.06.010.

Dorschel, B., Hebbeln, D., Rüggeberg, A., Dullo, C., 2007a. Carbonate budget of a cold-water coral carbonate mound: propeller mound, Porcupine Seabight. Int. J. Earth Sci. 96, 73–83. http://dx.doi.org/10.1007/s00531-005-0493-0.

Douarin, M., Elliot, M., Noble, S.R., Sinclair, D., Henry, L.-A., Long, D., Moreton, S.G., Murray Roberts, J., 2013. Growth of north-east Atlantic cold-water coral reefs and mounds during the Holocene: a high resolution U-series and 14C chronology. Earth Planet. Sci. Lett. 375, 176–187. http://dx.doi.org/10.1016/j.epsl.2013.05.023.

Douville, E., Sallé, E., Frank, N., Eisele, M., Pons-Branchu, E., Ayrault, S., 2010. Rapid and accurate U–Th dating of ancient carbonates using inductively coupled plasma-

quadrupole mass spectrometry. Chem. Geol. 272, 1–11. http://dx.doi.org/10.1016/j.chemgeo.2010.01.007.

Dullo, W.C., Flögel, S., Rüggeberg, A., 2008. Cold-water coral growth in relation to the hydrography of the Celtic and Nordic European continental margin. Mar. Ecol. Prog. Ser. 371, 165–176. http://dx.doi.org/10.3354/meps07623.

Ellett, D.J., Edwards, A., Bowers, R., 1986. The hydrography of the Rockall Channel—an overview. Proc. R. Soc. Edinb. Sect. B Biol. Sci. 88, 61–81. http://dx.doi.org/10.1017/S0269727000004474.

Flot, J.-F., Dahl, M., André, C., 2013. Lophelia pertusa corals from the Ionian and Barents seas share identical nuclear ITS2 and near-identical mitochondrial genome sequences. BMC Res. Notes 6, 144. http://dx.doi.org/10.1186/1756-0500-6-144.

Foubert, A., Henriet, J.P., 2009. Nature and Significance of the Recent Carbonate Mound Record: The Mound Challenger Code. vol. 126. Springer Science & Business Media, p. 350.

Foubert, A., Huvenne, V.A.I., Wheeler, A., Kozachenko, M., Opderbecke, J., Henriet, J.-P., 2011. The Moira Mounds, small cold-water coral mounds in the Porcupine Seabight, NE Atlantic: part B—evaluating the impact of sediment dynamics through high-resolution ROV-borne bathymetric mapping. Mar. Geol. 282, 65–78. http://dx.doi.org/10.1016/j.margeo.2011.02.008.

Frank, N., Freiwald, A., Correa, M.L., Wienberg, C., Eisele, M., Hebbeln, D., Van Rooij, D., Henriet, J.-P., Colin, C., van Weering, T., de Haas, H., Buhl-Mortensen, P., Roberts, J.M., De Mol, B., Douville, E., Blamart, D., Hatte, C., 2011. Northeastern Atlantic cold-water coral reefs and climate. Geology 39, 743–746. http://dx.doi.org/10.1130/G31825.1.

Frank, N., Paterne, M., Ayliffe, L., van Weering, T., Henriet, J.-P., Blamart, D., 2004. Eastern North Atlantic deep-sea corals: tracing upper intermediate water Δ14C during the Holocene. Earth Planet. Sci. Lett. 219, 297–309. http://dx.doi.org/10.1016/S0012-821X(03)00721-0.

Frank, N., Ricard, E., Lutringer-Paquet, A., van der Land, C., Colin, C., Blamart, D., Foubert, A., Van Rooij, D., Henriet, J.-P., de Haas, H., van Weering, T., 2009. The Holocene occurrence of cold water corals in the NE Atlantic: implications for coral carbonate mound evolution. Mar. Geol. 266, 129–142. http://dx.doi.org/10.1016/j.margeo.2009.08.007.

Freiwald, A., 2009. The white coral community. Oceanography 22, 58–74.

Hansen, B., Osterhus, S., 2000. North Atlantic nordic seas exchanges. Prog. Oceanogr. 45, 109–208. http://dx.doi.org/10.1016/S0079-6611(99)00052-X.

Henry, L.-A., Frank, N., Hebbeln, D., Wienberg, C., Robinson, L., van de Flierdt, T., Dahl, M., Douarin, M., Morrison, C.L., López, C.M., Rogers, A.D., Ruckelshausen, M., Roberts, J.M., 2014. Global ocean conveyor lowers extinction risk in the deep sea. Deep-Sea Res. I 88, 8–16.

Henry, L.-A., Navas, J.M., Hennige, S.J., Wicks, L.C., Vad, J., Murray Roberts, J., 2013. Cold-water coral reef habitats benefit recreationally valuable sharks. Biol. Conserv. 161, 67–70. http://dx.doi.org/10.1016/j.biocon.2013.03.002.

Holliday, N., Pollard, R.T., Read, J.F., Leach, H., 2000. Water mass properties and fluxes in the Rockall Trough, 1975–1998. Deep-Sea Res. I Oceanogr. Res. Pap. 47, 1303–1332. http://dx.doi.org/10.1016/S0967-0637(99)00109-0.

Horwitz, E.P., 1998. Extraction chromatography of actinides and selected fission products: principles and achievement of selectivity. International workshop on the application of extraction chromatography in radionuclide measurement. IRMM, Geel, pp. 9–10.

Howell, K.L., Huvenne, V., Piechaud, N., Robert, K., Ross, R.E., 2014. Analysis of biological data from the JC060 survey of areas of conservation interest in deep waters off north and west Scotland. JNCC Report No. 528.

Huvenne, V.A.I., 2011. Benthic habitats and the impact of human activities in Rockall Trough, on Rockall Bank and in Hatton Basin. RRS James Cook Cruise 60 Report, 09 May-12 Jun 2011, p. 133.

Huvenne, V.A.I., Masson, D.G., Wheeler, A.J., 2009a. Sediment dynamics of a sandy contourite: the sedimentary context of the Darwin cold-water coral mounds, Northern Rockall Trough. Int. J. Earth Sci. 98, 865–884. http://dx.doi.org/10.1007/s00531-008-0312-5.

Huvenne, V.A.I., Van Rooij, D., De Mol, B., Thierens, M., O'Donnell, R., Foubert, A., 2009b. Sediment dynamics and palaeo-environmental context at key stages in the challenger cold-water coral mound formation: clues from sediment deposits at the mound base. Deep-Sea Res. I Oceanogr. Res. Pap. 56, 2263–2280. http://dx.doi.org/10.1016/j.dsr.2009.08.003.

Johnson, C., Inall, M., Häkkinen, S., 2013. Declining nutrient concentrations in the northeast Atlantic as a result of a weakening subpolar gyre. Deep-Sea Res. I Oceanogr. Res. Pap. 82, 95–107. http://dx.doi.org/10.1016/j.dsr.2013.08.007.

Kobashi, T., Severinghaus, J.P., Brook, E.J., Barnola, J.-M., Grachev, A.M., 2007. Precise timing and characterization of abrupt climate change 8200 years ago from air trapped in polar ice. Quat. Sci. Rev. 26, 1212–1222. http://dx.doi.org/10.1016/j.quascirev.2007.01.009.

Larsson, A.I., Järnegren, J., Strömberg, S.M., Dahl, M.P., Lundälv, T., Brooke, S., 2014. Embryogenesis and larval biology of the cold-water coral lophelia pertusa. PLoS One 9, e102222. http://dx.doi.org/10.1371/journal.pone.0102222.

Lozier, M.S., Stewart, N.M., 2008. On the temporally varying northward penetration of Mediterranean overflow water and eastward penetration of Labrador sea water. J. Phys. Oceanogr. 38, 2097–2103. http://dx.doi.org/10.1175/2008JPO3908.1.

Masson, D., Bett, B., Billett, D.S., Jacobs, C., Wheeler, A., Wynn, R., 2003. The origin of deep-water, coral-topped mounds in the northern Rockall Trough, Northeast Atlantic. Mar. Geol. 194, 159–180. http://dx.doi.org/10.1016/S0025-3227(02)00704-1.

McCulloch, M., Taviani, M., Montagna, P., López Correa, M., Remia, A., Mortimer, G., 2010. Proliferation and demise of deep-sea corals in the Mediterranean during the younger dryas. Earth Planet. Sci. Lett. 298, 143–152. http://dx.doi.org/10.1016/j.epsl.2010.07.036.

Moran, S.B., Hoff, J.A., Buesseler, K.O., Edwards, R.L., 1995. High Precision and Z3ZTh in the Norwegian Sea and Denmark by Thermal Ionization Mass Spectrometry. 22, 2589–2592.

Pons-Branchu, E., Douville, E., Roy-Barman, M., Dumont, E., Branchu, P., Thil, F., Frank, N., Bordier, L., Borst, W., 2014. A geochemical perspective on Parisian urban history based on U–Th dating, laminae counting and yttrium and REE concentrations of recent carbonates in underground aqueducts. Quat. Geochronol. 24, 44–53. http://dx.doi.org/10.1016/j.quageo.2014.08.001.

Raddatz, J., Rüggeberg, A., Liebetrau, V., Foubert, A., Hathorne, E.C., Fietzke, J., Eisenhauer, A., Dullo, W.-C., 2014. Environmental boundary conditions of cold-water coral mound growth over the last 3 million years in the Porcupine Seabight, Northeast Atlantic. Deep-Sea Res. II Top. Stud. Oceanogr. 99, 227–236. http://dx.doi.org/10.1016/j.dsr2.2013.06.009.

Rasmussen, T., Bäckström, D., Heinemeier, J., Klitgaard-Kristensen, D., Knutz, P., Kuijpers, A., Lassen, S., Thomsen, E., Troelstra, S., van Weering, T.C., 2002. The faroe–shetland gateway: late quaternary water mass exchange between the Nordic seas and the northeastern Atlantic. Mar. Geol. 188, 165–192. http://dx.doi.org/10.1016/S0025-3227(02)00280-3.

Reimer, P.J., Bard, E., Bayliss, A., Beck, J.W., Blackwell, P.G., Ramsey, C.B., 2013. IntCal13 and Marine13 radiocarbon age calibration curves 0–50,000 years cal BP. Radiocarbon 55, 1869–1887. http://dx.doi.org/10.2458/azu_js_rc.55.16947.

Roberts, J.M., Wheeler, A.J., Freiwald, A., 2006. Reefs of the deep: the biology and geology of cold-water coral ecosystems. Science 312, 543–547. http://dx.doi.org/10.1126/science.1119861.

Roberts, J.M., Wheeler, A., Freiwald, A., Cairns, S., 2009. Cold Water Corals: The Biology and Geology of Deep-Sea Coral Habitats. Cambridge University Press, New York.

Smith, W.H.F., Sandwell, D.T., 1997. Global seafloor topography from satellite altimetry and ship depth soundings. Science 277, 1957–1962.

Soulsby, R., 1997. Dynamics of Marine Sands. A manual for practical applications. Thomas Telford Publications, London, p. 249.

Staines-Urías, F., Kuijpers, A., Korte, C., 2013. Evolution of subpolar North Atlantic surface circulation since the early Holocene inferred from planktic foraminifera faunal and stable isotope records. Quat. Sci. Rev. 76, 66–81. http://dx.doi.org/10.1016/j.quascirev.2013.06.016.

Thierens, M., Browning, E., Pirlet, H., Loutre, M.-F., Dorschel, B., Huvenne, V.A.I., Titschack, J., Colin, C., Foubert, A., Wheeler, A.J., 2013. Cold-water carbonate mounds as unique palaeo-archives: the Plio-Pleistocene challenger mound record (NE Atlantic). Quat. Sci. Rev. 73, 14–30. http://dx.doi.org/10.1016/j.quascirev.2013.05.006.

Van der Land, C., Eisele, M., Mienis, F., de Haas, H., Hebbeln, D., Reijmer, J.J.G., van Weering, T.C.E., 2014. Carbonate mound development in contrasting settings on the Irish margin. Deep-Sea Res. II Top. Stud. Oceanogr. 99, 297–306. http://dx.doi.org/10.1016/j.dsr2.2013.10.004.

Van Oevelen, D., Duineveld, G., Lavaleye, M., Mienis, F., Soetaert, K., Heip, C.H.R., 2009. The cold-water coral community as hotspot of carbon cycling on continental margins: a food-web analysis from Rockall Bank (northeast Atlantic). Limnol. Oceanogr. 54, 1829–1844. http://dx.doi.org/10.4319/lo.2009.54.6.1829.

Vogler, S., Scholten, J., Rutgers van der Loeff, M., Mangini, A., 1998. 230Th in the eastern north atlantic: the importance of water mass ventilation in the balance of230Th. Earth Planet. Sci. Lett. 156, 61–74. http://dx.doi.org/10.1016/S0012-821X(98)00011-9.

Wheeler, A.J., Ferdelman, T., Freiwald, A., Hebbeln, D., Henriet, J.P., 2007. Cold-Water Coral Ecosystem Functioning through Time in the Deep Sea: The example of cold-water coral carbonate mounds in the northeast Atlantic (from IODP307 to EuroMARC - CARBONATE). 9.

Wheeler, A.J., Kozachenko, M., Henry, L.-A., Foubert, A., de Haas, H., Huvenne, V.A.I., Masson, D.G., Olu, K., 2011. The Moira Mounds, small cold-water coral banks in the Porcupine Seabight, NE Atlantic: part A—an early stage growth phase for future coral carbonate mounds? Mar. Geol. 282, 53–64. http://dx.doi.org/10.1016/j.margeo.2010.08.006.

Wheeler, A.J., Kozachenko, M., Masson, D.G., Huvenne, V.A.I., 2008. Influence of benthic sediment transport on cold-water coral bank morphology and growth: the example of the Darwin Mounds, north-east Atlantic. Sedimentology 55, 1875–1887. http://dx.doi.org/10.1111/j.1365-3091.2008.00970.x.

White, M., 2007. Benthic dynamics at the carbonate mound regions of the Porcupine Sea Bight continental margin. Int. J. Earth Sci. 96, 1–9. http://dx.doi.org/10.1007/s00531-006-0099-1.

Wienberg, C., Hebbeln, D., Fink, H.G., Mienis, F., Dorschel, B., Vertino, A., Correa, M.L., Freiwald, A., 2009. Scleractinian cold-water corals in the Gulf of Cádiz—first clues about their spatial and temporal distribution. Deep-Sea Res. I Oceanogr. Res. Pap. 56, 1873–1893. http://dx.doi.org/10.1016/j.dsr.2009.05.016.